Theor Chem Acc (2009) 123:487–500
DOI 10.1007/s00214-009-0569-1

REGULAR ARTICLE

Study of water clusters in the $n = 2$–34 size regime, based on the ABEEM/MM model

Ping Qian · Li-nan Lu · Wei Song · Zhong-zhi Yang

Received: 13 February 2009 / Accepted: 10 April 2009 / Published online: 30 April 2009

Abstract Various properties of water clusters in the $n = 2$–34 size regime with the change of cluster size have been systemically explored based on the newly developed flexible-body and charge-fluctuating ABEEM/MM water potential model. The ABEEM/MM water model is to take ABEEM charges of all atoms, bonds, and lone-pairs of water molecules into the intermolecular electrostatic interaction term in molecular mechanics. The computed correlating properties characterizing water clusters $(H_2O)_n$ ($n = 2$–34) include optimal structures, structural parameters, ABEEM charge distributions, binding energies, hydrogen bonds, dipole moments, and so on. The study of optimal structures shows that the ABEEM/MM model can correctly predict the following important structural features, such as the transition from two-dimensional (from dimer to pentamer) to three-dimensional (for clusters larger than the hexamer) structures at hexamer region, the transition from cubes to cages at dodecamer $(H_2O)_{12}$, the transition from all-surface (all water molecules on the surface of the cluster) to one water-centered (one water molecule at the center of the cluster, fully solvated) structures at $(H_2O)_{17}$, the transition from one to two internal molecules in the cage at $(H_2O)_{33}$, and so on. The first three structural transitions are in good agreement with those obtained from previous work, while the fourth transition is different from that identified by Hartke. Subsequently, a systematic investigation of structural parameters, ABEEM charges, energetic properties, and dipole moments of water clusters with increasing cluster size can provide important reference for describing the objective trait of hydrogen bonds in water cluster system, and also provide a strong impetus toward understanding how the water clusters approach the bulk limit.

Keywords ABEEM/MM · Water clusters · Hydrogen bond

1 Introduction

"Water clusters", groups of water molecules held together by hydrogen bonds, have been the subject [1] of a large number of experimental and theoretical investigations because of their importance in understanding cloud and ice formation, solution chemistry, and a lot of biochemical processes [2]. Water clusters display a variety of interesting behaviors and are, therefore, worthy of basic research for their own sake. In particular, clusters can be considered a bridge between the gas phase and the condensed phases, and therefore, evolution toward condensed phase structure and dynamics as a function of size is of interest.

So far, the properties of small water clusters $(H_2O)_n$ ($n = 2$–6) have been extensively studied experimentally [3–10] and theoretically [11–23]. A number of previous

Electronic supplementary material The online version of this article (doi:10.1007/s00214-009-0569-1) contains supplementary material, which is available to authorized users.

P. Qian (✉)
Chemistry and Material Science Faculty,
Shandong Agricultural University,
271018 Tai'an, People's Republic of China
e-mail: qianp@sdau.edu.cn; zzyang@lnnu.edu.cn

L. Lu · Z. Yang
Chemistry and Chemical Engineering Faculty,
Liaoning Normal University,
116029 Dalian, People's Republic of China

W. Song
Tai'an Centers for Disease Control and Prevention,
271000 Tai'an, People's Republic of China

studies [3, 4, 11] showed that the most stable structure of water dimer was of the C_s symmetry, and that it had a single hydrogen bond with strength of 5.44 ± 0.7 kcal/mol. Recently, based on more high quality first principles electronic structure calculations [21] at the second order perturbation level of theory, the corresponding binding energy for the dimer is about 5.0 kcal/mol. At the same time, these studies demonstrated conclusively a cyclic structure for $n = 3$–5 and a transition from two-dimensional (2D) cyclic structure to three-dimensional (3D) structure at $n = 6$. For the octamer, two very stable cubic structures (S_4 and D_{2d}) were predicted [24–30]. The stable symmetric cube structures of the octamer were reported for the $(H_2O)_8$-benzene cluster [31] and for water clusters with the phenol chromophore [32]. Measurement of size selected infrared spectra of $(H_2O)_n$ in the $n = 7$–10 range, in conjunction with calculations, resulted in assignment to single cage structures. The $n = 7$–10 minimum energy structures can be viewed as derived from the octamer cube, by addition or subtraction of molecules [33–35].

To the best of our knowledge, most of the available experimental data for neutral $(H_2O)_n$ ($n > 10$) clusters pertain to distributions of cluster sizes rather than to a single known size [36–43], although there are interesting current advances in spectroscopy of size-selected water clusters doped with an Na atom [43]. For the $n = 11$–30 size range, considerable insight has been gained from theoretical studies [16, 18, 20, 22, 23, 29, 44–70]. For instance, Tsai and Jordan [44] found that the TIP4P potential for water clusters favored a cuboid geometry over the hollow cage for $n = 12$, 16, and 20. Their MP2 calculations confirmed that the cuboid geometry was the most stable for $n = 12$. Additionally, ab initio calculations by Sremaniak et al. [45] supported the stacked cubic structure of $D_{2d}D_{2d}$ symmetry over the stacked cyclic hexamers of S_6 symmetry. MNDO-PM3 calculations [46] also suggested the cuboid geometries to be the most stable for $(H_2O)_{12}$ and $(H_2O)_{16}$. Kirschner and Shields [47] predicted cuboids and fused pentameric structures to be the most stable for $(H_2O)_{20}$. However, it is common accepted for potential model that eventually the cagelike structures will prevail over cubes, but the size of the cluster at which this transition occurs is still debated. Subsequently, we find that such a transition occurred at different cluster sizes, depending on the water model. For the SPC/E model [71] this transition occurs for $(H_2O)_n$ at $n = 20$. For the POL1 [72] model, the cage appears at $n = 12$. In the Stillinger and David's polarizable model [73, 74] cubes do not appear even at the $n = 8$ size. Interestingly, on the basis of his semiempirical calculations at the INDO level, Khan [48] also concluded that stacked cubes are unlikely to be formed and that cage structures are more likely as the cluster size increases. He has proposed [49–52] several different cage structures for $(H_2O)_n$ ($n = 24$–35). Some of them are fused and have free water molecules inside the cage. Day et al. [53] used simulated annealing methods with the effective fragment potential to locate the most stable structures for the water clusters $(H_2O)_n$ with $n = 6$, 8, 10, 12, 14, 16, 18, and 20. Most recently, structural evolution as a function of size in the $n = 2$–30 range regime was addressed systematically by Hartke [60–62] for the TIP4P [75] and TTM2-F [18–20, 22, 23, 30] potentials. Clusters at the low end of this size range have been described as "all surface". Increase in size is marked by appearance of three-dimensional "centered cage" forms with one or two 4-coordinated core molecules in the interior. Recently, Xantheas et al. [66] have confirmed the existence of the transitional size regime from electronic structure calculations for $(H_2O)_n$ ($n = 17$–21). Moreover, a number of theoretical studies focused on the simulations of melting transition in water clusters [67, 68, 73, 74] and on the investigations of special structures which were proposed to be particularly interesting and/or stable.

However, even with all this activity in the study of clusters during the last decades, there is still a considerable lack of understanding of the transitions from the properties and structures of the small-, intermediate-sized clusters to those of the large-sized clusters. In particular, starting from sizes of small water clusters, it is more meaningful for any potential to investigate the evolution of general structure, energy, hydrogen bond and dipole moment as functions of size. ABEEM/MM force field [76–84] is a newly developed flexible body and fluctuating charge potential model. In this model, a water molecule is described by seven-point (7P) charges, including three atom charges, two bond charges and two lone-pair electron charges (TIP7P), which can reflect the charge distribution and polarization properly. Furthermore, in characterizing binding energy, geometry, hydrogen-bonding energies, as well as dynamic properties, the ABEEM/MM fluctuating charge potential model gives quite accurate predictions, and the results are comparable with ab initio results for small water clusters [76, 77], ion–water clusters [78], organic and biological molecules [79–81], and the aqueous solutions [82–84].

The information of water clusters for $n > 22$ is very little. The purpose of this paper is to explore low-energy structures of $(H_2O)_n$ in the $n = 2$–34 size regime, and further present the variation trends of various properties characterizing water clusters (including optimal structures, structural parameters, hydrogen bonds, charge distributions, interaction energies, dipole moments, and so on) with the ABEEM/MM model.

The remainder of this article is organized as follows. In Sect. 2, we give the descriptions of ABEEM/MM water model and optimization method. In Sect. 3, we give the results and discussions of various properties of water

clusters in the $n = 2$–34 size regime. Finally, the conclusion is briefly given in Sect. 4.

2 Methodology

2.1 ABEEM/MM water model

The ABEEM/MM water model assumes that the water molecule is composed of seven charge centers, including three atoms, two bonds and two lone-pair electrons. According to the equilibrium geometry of a water molecule (Fig. 1), the bond length of O–H and the bond angle of H–O–H are set to their experimental values, 0.9572 Å and 104.52°, respectively, and the lone-pair electron center is 0.74 Å far from the oxygen nucleus with an intervening angle of 109.47°. According to the ABEEM/MM model, the potential energy of pure water system is written as

$$E = \sum_{\text{bonds}} E_{\text{b}} + \sum_{\text{angles}} E_{\theta} + \sum_{\text{non-bonded}} (E_{\text{vdw}} + E_{\text{elec}}), \qquad (1)$$

where E_{b}, E_{θ}, E_{vdw}, and E_{elec} stand for the energies of individual bond stretching, angle bending, van der Waals, and electrostatic interaction, respectively. The cross terms, like stretch-bend coupling, etc., are omitted in Eq. 1. The above equation can be concretely expressed as follows:

$$\begin{aligned} E = {} & \sum_{\text{bonds}} D[\mathrm{e}^{-2\alpha(r-r_{\text{eq}})} - 2\mathrm{e}^{-\alpha(r-r_{\text{eq}})}] + \sum_{\text{angles}} K_{\theta}(\theta-\theta_{\text{eq}})^2 \\ & + \sum_{i}\sum_{j\neq i}\left\{\sum_{a}\sum_{b}\varepsilon_{ia,jb}\left[\left(\frac{r_{\min_{ia,jb}}}{r_{ia,jb}}\right)^{12} - 2\times\left(\frac{r_{\min_{ia,jb}}}{r_{ia,jb}}\right)^{6}\right]\right. \\ & + \sum_{\substack{H\in i \\ (H,\text{lp in HBIR})}}\sum_{\text{lp}\in \text{j}} k_{iH,j(\text{lp})}(R_{iH,j(\text{lp})})\frac{q_{iH}q_{j(\text{lp})}}{R_{iH,j(\text{lp})}} \\ & + k\left[\frac{1}{2}\sum_{a}\sum_{b}\frac{q_{ia}q_{jb}}{R_{ia,jb}} + \frac{1}{2}\sum_{a-b}\sum_{g-h}\frac{q_{i(a-b)}q_{j(g-h)}}{R_{i(a-b),j(g-h)}}\right. \\ & + \frac{1}{2}\sum_{\text{lp}}\sum_{\text{lp}'}\frac{q_{i(\text{lp})}q_{i(\text{lp}')}}{R_{i(\text{lp}),\text{j}(\text{lp}')}} + \sum_{g-h}\sum_{a}\frac{q_{ia}q_{j(g-h)}}{R_{ia,j(g-h)}} \\ & \left.\left. + \sum_{\substack{a \\ (a\neq H,H\text{ in HBIR} \\ \text{and lp not in HBIR})}}\sum_{\text{lp}}\frac{q_{ia}q_{j(\text{lp})}}{R_{ia,j(\text{lp})}} + \sum_{\text{lp}}\sum_{a-b}\frac{q_{i(a-b)}q_{j(\text{lp})}}{R_{i(a-b),j(\text{lp})}}\right]\right\} \end{aligned} \qquad (2)$$

In Eq. 2, the Morse potential is used to represent the O–H bond stretching E_{b}, where the O–H bond dissociation energy D is 529.6 kcal/mol and α is related to the bond force constant ($\alpha = \sqrt{f_{\text{b}}/2D}$, f_{b} is the bond force constant), and r_{eq} is the equilibrium bond length 0.9572 Å. The harmonic potential is employed to represent the H–O–H angle bending

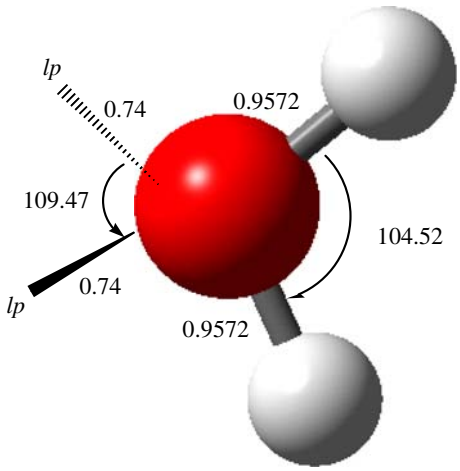

Fig. 1 The structure of monomer water by the ABEEM/MM model

E_{θ}, where the angle force constant k_{θ} is 34.05 kcal/(mol × deg^2) and θ_{eq} is the equilibrium bond angle 104.52°. Lennard–Jones interaction E_{vdw} between water molecules involves oxygen–oxygen, oxygen–hydrogen, and hydrogen–hydrogen interactions, where $\varepsilon_{ia,jb}$ and $r_{\min_{ia,jb}}$ are the Lennard–Jones well depth and minimum energy distance for the interaction between atom a belonging to water molecule i and atom b belonging to water molecule j, respectively. For the oxygen–hydrogen interaction, the ε_{OH} equals the geometric mean of the values for the two pure species well depth and the minimum energy distance $r_{\min_{\text{OH}}}$ is given as the arithmetic mean, viz., $\varepsilon_{\text{OH}} = \sqrt{\varepsilon_{\text{OO}}\varepsilon_{\text{HH}}}$, and $r_{\min_{\text{OH}}} = \frac{1}{2}(r_{\min_{\text{OO}}} + r_{\min_{\text{HH}}})$. The electrostatic interaction E_{elec} is calculated by using the ABEEM [85–90] charges, where q is the charge on every site of a water molecule. For example, q_a, q_{a-b}, and q_{lp} are the partial charges of atom a, bond a–b, and lone-pair electron lp, respectively, in which the bond charge q_{a-b} is placed on the point that partitions the bond length according to the ratio of covalent atomic radii of atom a and atom b. R is the distance between charge sites, for example, $R_{a,b}$, $R_{a-b,g-h}$, and $R_{\text{lp,lp}'}$ are the distance between atom a and atom b, the distance between bond a–b and bond g–h, and the distance between lone-pair electron lp and lone-pair electron lp′, and so on. Parameter k is an overall correction coefficient in this model. Parameter $k_{i\text{H},j(\text{lp})}$ $R_{(i\text{H},j(\text{lp}))}$ is related to the separation between the hydrogen atom belonging to water molecule i and the lone-pair electron belonging to water molecule j in the hydrogen bond interaction region (HBIR). The detailed derivation and the procedures of parameterization for the ABEEM/MM water model can be found in Yang et al. [76]. When there is a change of bond, angle, and relative position of molecules, we recalculate the charges by ABEEM method [85–90], and recalculate the total energy by Eq. 2. In the calculations, we only considered a charge neutrality constraint on each water molecule and there is no charge transfer between the

molecules and the effective chemical potentials of an atom, a bond and a lone-pair electron only within a molecule are set equal.

2.2 Optimization method

In ABEEM/MM calculations, we start with our ab initio geometries at the HF/6-31G(d) level and perform local energy minimization with the limited memory BFGS quasi-Newton nonlinear optimization method [91]. All possible structures are fully optimized taking into account the positions of all atoms within the cluster.

In view of the large number of possible geometries for the larger clusters, there would be several minima on a shallow potential energy surface, and it becomes extremely difficult to locate the true energy minimum for each cluster. Therefore, it is worth noting that we present the results not as the global minima for the clusters but as an investigation of several ordered sampling structures. That is, we cannot guarantee that we have found the global minima of the clusters, but we are interested in the progression of the ordered structures which are the relatively most stable in energy for each cluster, and then to further understand the characteristics of hydrogen bonds. These water aggregates are built on a step-by-step basis starting from the dimer ($n = 2$) and up to $(H_2O)_{34}$ cluster in the light of different component forms. These clusters are composed of cubic octamer-like subunits [24, 25, 92], tubes of five- and/or six-membered water rings [93], flat sandwich-like structures [94], large spheroid single cages [49–52], fused cage structures [49–52], and water-centered cage structures with one or two 4-coordinated core molecules in the interior [60–62].

3 Results and discussions

3.1 Optimal structures of $(H_2O)_n$ ($n = 2$–34) clusters

Structurally the water clusters could be classified into two broad categories, viz., 2D structures (for example, ring structure) and 3D structures (such as, cage, prism, or cube structure, and so on). Main low-lying energy conformers of water clusters $(H_2O)_n$ ($n = 2$–34), binding energies, hydrogen bonds number, and dipole moments optimized and calculated by the ABEEM/MM model are shown in Figs. 2, 3, 4, 5, and other low-lying energy conformers and related information are available in the electronic supplementary material. Figures 2, 3, 4, 5 further confirm and reflect the following important structural features:

(1) Small clusters (for $n < 6$) have 2D conformers, while large clusters (for $n > 6$) have 3D conformers. The transition from 2D to 3D structures at hexamer region, which has been demonstrated by early work [95], is correctly reflected in the present study, and the detailed descriptions are elucidated in Sect. 3.2 based on the change of structural parameters. It should be noted that in the case of ring pentamer the hydrogen bonding orientation corresponds to the most energetically favorable conformation among the 2D structures. Thus, with increasing cluster size, the energy gain of the hexamer relative to the pentamer becomes minimal, so the hexamer structures are at the border between 2D and 3D conformations, resulting in diverse isoenergetic structures [96] such as ring, book, and so on. These diverse isoenergetic hexamer conformers would play an important role in entropy, and so be responsible for various phase transitions of ice as well as water. This would be related to the magic number of six in various water-containing molecular systems as well as ice.

(2) The transition from cubes to cages is predicted by the ABEEM/MM model at $(H_2O)_n$ ($n = 12$), and the abundance of pentamers increases with increasing cage-like character. This transition is in good agreement with that identified by the POL1 model [45]. In Fig. 3, the relatively most stable structure of $(H_2O)_{12}$ does not occur at the double cube structures (such as $D_{2d}D_{2d}$, $D_{2d}S_4$, S_4S_4), but occurs at the cagelike structure of D_3 symmetry.

Rather than viewing the clusters as monomer units connected via hydrogen bonds, they can be viewed as small cluster units fused together to form a larger cluster. The double-cube $(H_2O)_{12}$ clusters, for instance, can be thought of as a fusion of two book hexamers and seven tetramer units. The D_3 structure for $(H_2O)_{12}$ cluster can likewise be thought of as a fusion of two ring hexamers and six tetramer units. To better understand the $(H_2O)_{12}$ cluster with D_3 symmetry, we paid attention to the correlated information about $(H_2O)_6$. If the hydrogen bond that forms the "binding" of book hexamer is broken, then the ring structure is obtained. Thus for $(H_2O)_{12}$, the topologies of the double-cube and D_3 cage-like structures are very similar if viewed from the perspective of fusing two groups of hexamers. To go from a double-cube $D_{2d}S_4$ structure to the D_3 cage-like structure, it would give rise to two effects: first, the two hydrogen bonds forming the "binding" of the two book hexamers must be broken, and breaking hydrogen bonds somewhat destabilize the D_3 cagelike structure; second, when the above two hydrogen bonds are broken, the ring strain reduces because the number of four-membered rings decreases by four and the number of six-membered rings increases by two, and this reduction degree somewhat stabilizes the D_3 cagelike structure. As a final result, of the above two factors, D_3 cagelike structure is more stable than the double-cube $D_{2d}S_4$ structure by 5.90 kcal/mol. Therefore, breaking hydrogen bonds somewhat destabilize the structure, but this effect is compensated by a reduction in ring strain. In other words, there is a balance between the numbers of tetramers which result in

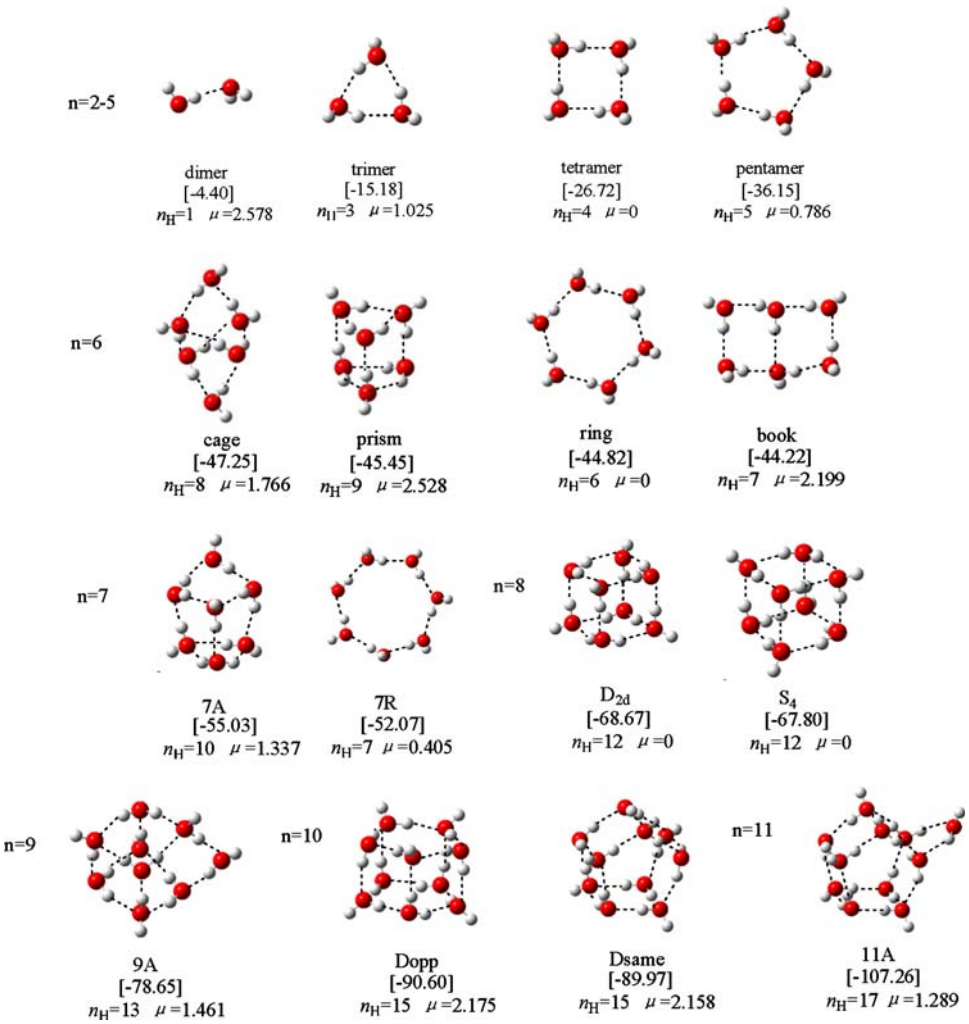

Fig. 2 Various low energy structures, binding energies (BE) in kcal/mol, the hydrogen bonds number (n_H), and dipole moments (μ) in Debye of $(H_2O)_{2-11}$ clusters optimized and calculated by the ABEEM/MM model

more hydrogen bonds and the numbers of pentamers and hexamers which alleviate some ring strain since perfect pentamers and hexamers allow for better accommodation of the hydrogen bonds than does the tetramer. Indeed, the abundance of pentamers, in particular, increases with increasing cagelike character. For example, in going from $(H_2O)_{12}$ to $(H_2O)_{16}$ (Fig. 3), the number of five-membered rings increases from zero to four.

(3) A size-dependent transition from all-surface to one water-centered structures at $n = 17$, which has been reported by Hartke [60–62], is also further reflected and correctly predicted in the present study. At the same time, there is an evident alternation occurring between internally solvated ($n = 17, 19, 21, 23, 26–29$) and all-surface ($n = 18, 20, 22, 24–25, 30–32$) configurations for the relatively most stable structures with the ABEEM/MM model. This alternation is similar to the conclusion reached by Xantheas [66] from electronic structure calculations for $(H_2O)_n$, $n = 17–21$.

(4) As the cage interior gets larger and larger, a transition from one to two internal molecules in the cage is predicted at $n = 33$. In comparison, Hartke [60–62] has reported this kind of structural transition at $n = 27–28$. Just as Hartke [60–62] has mentioned, as a final note on the larger clusters, it should be pointed out that none of their structural features bears any resemblance to typical structural patterns of any of the crystalline bulk ice forms. That is, all of these clusters should be characterized as amorphous. This is in accord with experimental observations on water clusters from this size range to far larger ones (with size-preference but without single size-selection) [97, 98].

(5) The results for the water clusters $(H_2O)_n$ ($n = 12, 18, 24, 30$) show that the relatively most stable structures of the clusters present a certain regular behavior. That is, the relatively most stable structures all have the ring hexamers as building units with opposite hydrogen bond orientation.

3.2 Structural parameters of $(H_2O)_n$ ($n = 2–34$) clusters

In addition to the above-mentioned structural features, it is very interesting to investigate the changes of structural parameters. It is noticeable that in this paper the mean

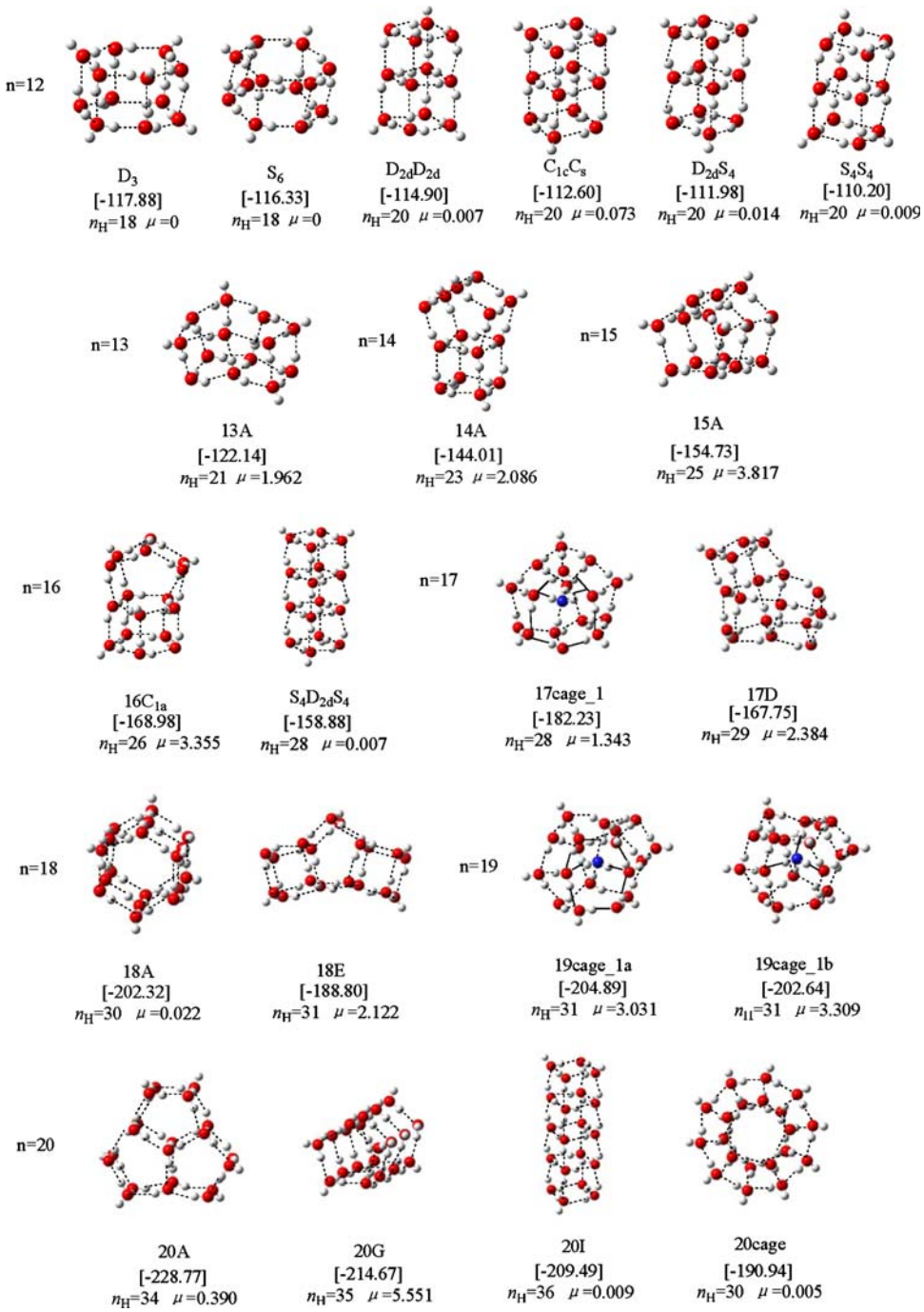

Fig. 3 Same as Fig. 2, for $(H_2O)_{12–20}$

values of structural parameters are not for thermal fluctuations of geometries or averages of a delocalized quantum state, but just for a single equilibrium configuration.

Figure 6 shows a sharp transition of the structural parameters at hexamer region predicted by the ABEEM/MM model. The mean value $R(O\cdots H)_{av}$ decreases with increasing n for $n < 6$. However, as the structure changes from the cyclic planar (2D) to 3D structure, the $R(O\cdots H)_{av}$ increases drastically. In the hexamer, the $R(O\cdots H)_{av}$ value of ring structure shows 1.86 Å, but those of book, cage, and prism structures show 1.91, 1.98 and 2.03 Å, respectively. Then, the values are somewhat steady around 1.94 Å for $n > 6$. This structural information is also well reflected in $R(O\cdots O)_{av}$. For $n < 6$, the mean values $\angle(OHO)_{av}$ decrease rapidly from dimer to trimer, and then those of pentamer and ring hexamer have few difference. However, for $n > 6$, the values of $\angle(OHO)_{av}$ take on rapid downtrend. In the region of hexamer, the values of $\angle(OHO)_{av}$ for ring and prism structures are 174.88° and 152.23°, respectively, while those of $\angle(OHO)_{av}$ for book and cage structures are

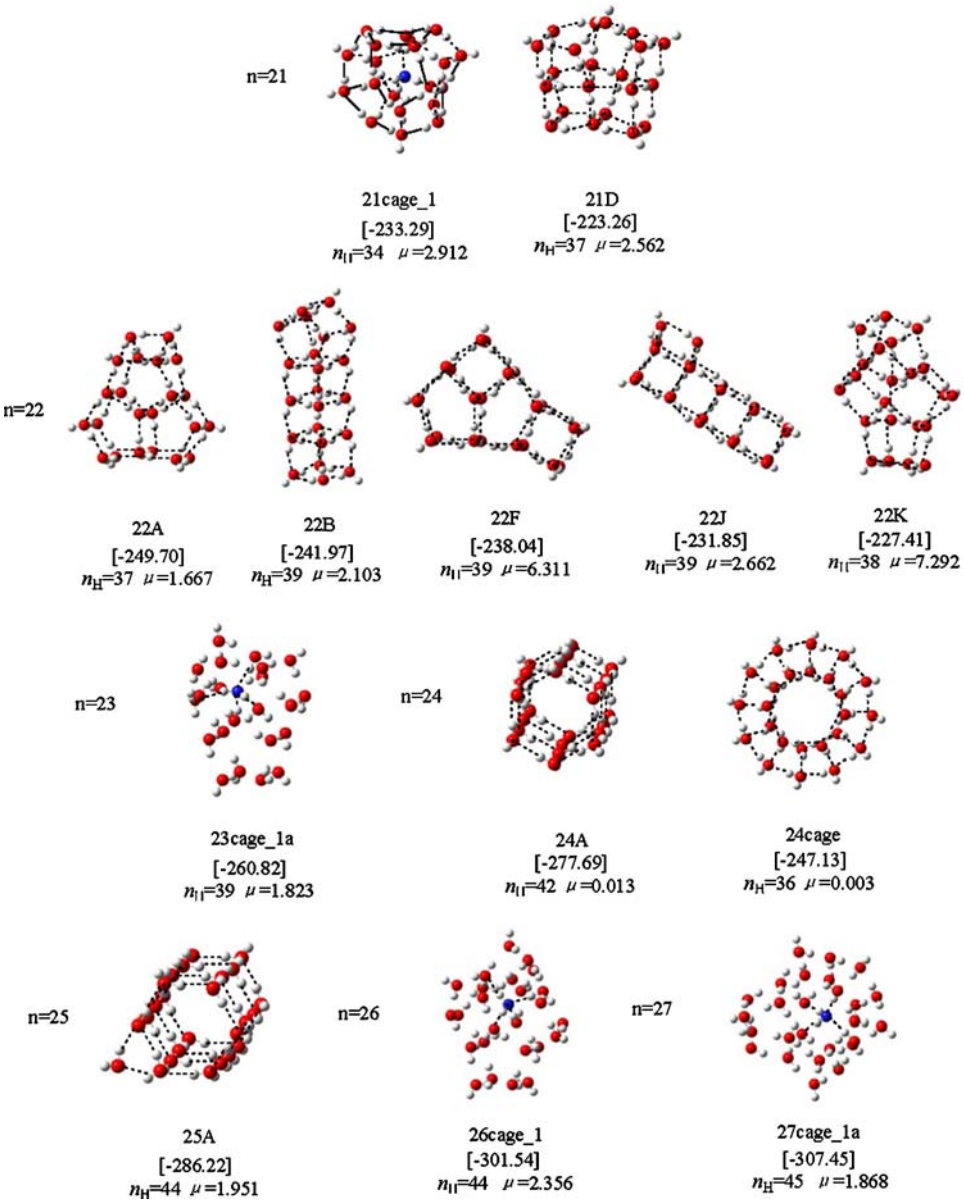

Fig. 4 Same as Fig. 2, for $(H_2O)_{21–27}$

166.42° and 158.55°, respectively, falling in the range between 174.88° and 152.23°. Thus, it can be seen that the ABEEM/MM model can correctly reflect the fact of transition from 2D cyclic to 3D structure in the hexamer region. It is just as Kim has reported [96], viz., the ring and prism conformers exhibit the characteristics of genuine 2D and 3D structures, respectively, while the book conformer is 2D like with some 3D characteristics, and the cage conformer is 3D like with some 2D characteristics.

Figure 7 shows the mean value $R(O\cdots H)_{av}$, $R(O–H)_{av}$, $R(O–H_b)_{av}$, $R(O\cdots O)_{av}$, $\angle(OHO)_{av}$ and $\angle(HOH)_{av}$ along with their variations in the form of vertical bars for the relatively most stable structures of $(H_2O)_n$ (n = 2–34) clusters. There are two types of hydrogen atoms in water clusters: one is referred to as "free hydrogen (H_f)" that is not involved in a hydrogen bond, and $R(O–H_f)$ represents the distance between oxygen and free hydrogen atom in water molecule; the other is referred to as "bridged hydrogen (H_b)" that is involved in a hydrogen bond, and $R(O–H_b)$ represents the distance between oxygen and bridged hydrogen atom in water molecule. In Fig. 7a, when n increases from two to five, the mean value $R(O\cdots H)_{av}$ decreases. However, when n = 6–34, $R(O\cdots H)_{av}$ increases drastically and is steady around some value. Similar structural information is also reflected in $R(O\cdots O)_{av}$ (Fig. 7c). The $R(O\cdots H)$ values are in the vicinity of 1.950 Å, falling in the expected range [99] of 1.70–2.45 Å. In Fig. 7b, the $R(O–H_b)$ values are different for the different hydrogen bonds in the relatively most stable conformers of the clusters, but the $R(O–H_b)_{av}$ values are all in the vicinity of 0.960 Å. Characteristically, the $R(O–H_b)$ values are larger than the $R(O–H_f)$

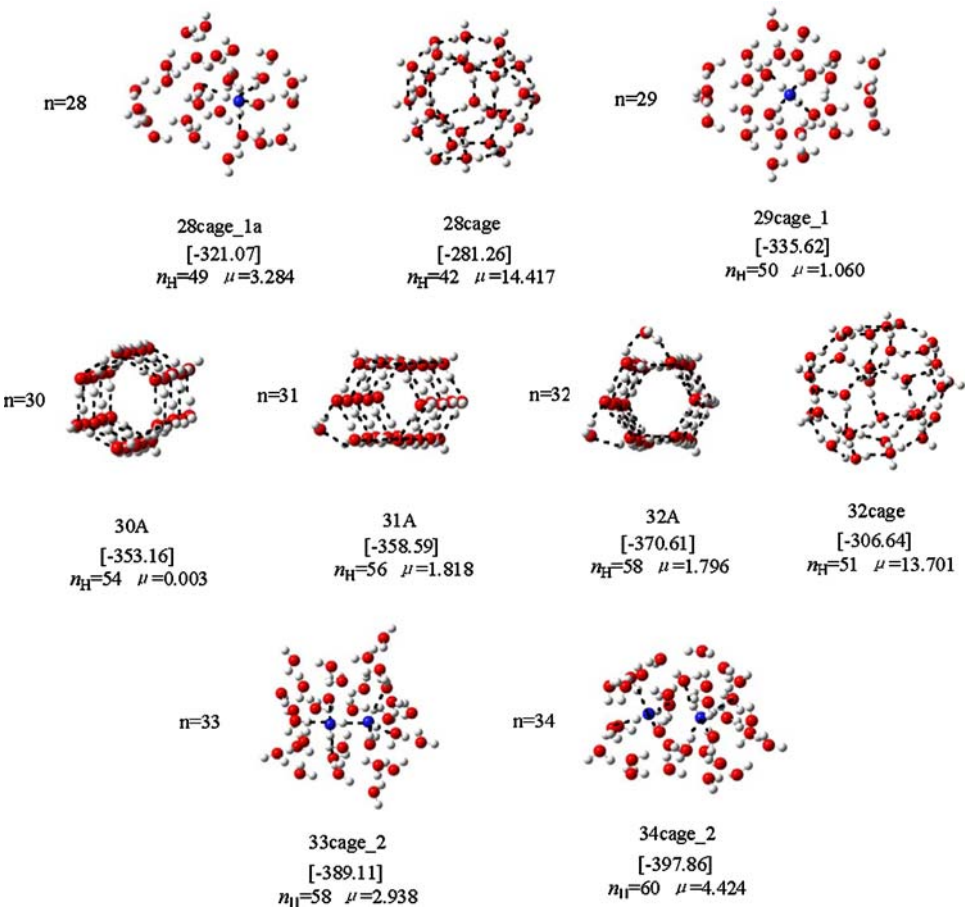

Fig. 5 Same as Fig. 2, for $(H_2O)_{28–34}$

values, as has been known for all of the hydrogen bonds in the literature. For the $n = 2$–5 ring clusters, there are only single-donor (sd) hydrogen bonds, whereas for $n \geq 6$, there are sd as well as double-donor (dd) hydrogen bonds. Figure 7d confirms previous review [29] that the $R(O–H_b)_{av}$ values for dd hydrogen bonds are slightly shorter than those for sd hydrogen bonds, and tests the reasonableness of the ABEEM/MM model. Figure 7e deals with the relationship between the angle ∠OHO value of H-bonded three atoms and the cluster size for $n = 2$–34. Because most of the hydrogen bonds are not exactly linear (∠OHO ~ 135°–176°), the distance $R(O\cdots O)_{av}$ is around 2.871 Å, slightly less than the sum of $R(O–H_b)_{av}$ and $R(O\cdots H)_{av}$. Moreover, the ABEEM/MM model also predicts the variation tendency of bend angle ∠HOH of the individual water molecules in the cluster with an increase in cluster size (Fig. 7f). The results show that when the cluster size increases, the mean values $\angle(HOH)_{av}$ fluctuate about 103.89°, less than the isolated monomer bend angle 104.52°.

3.3 ABEEM charge distributions

In this section, a cluster structure is arbitrarily chosen to study the ABEEM charge distributions. Take the relatively most stable structure of $(H_2O)_{17}$, for example, and the charges are listed in Table 1. For the model water, ABEEM/MM model [76] gives the explicitly quantitative charges of all atoms, bonds, and lone-pair electrons: the positive charges located on the O atom (0.1125) and H atoms (0.2897) are balanced by the negative charges located on the O–H bonds (−0.1552) and the lone-pair electrons (–0.1908). When water molecules interact with each other, the charges of all sites for each cluster are different from an isolated water, which is consequential upon environment change, i.e., for an isolated water, no other molecule affects its electron cloud, but for a cluster, which is composed of many water molecules, the different position of water molecule relative to another water molecule affects the redistribution of the electron cloud. Moreover, the intermolecular hydrogen bonds between water and water also directly influence the charge distribution. It is to be mentioned further that in the water clusters, there are four kinds of water molecules, viz., singe proton donor-single acceptor ("da"), single donor-double acceptor ("daa"), double donor-single acceptor ("dda"), and double donor-double acceptor ("ddaa").

Through analyzing the data in Table 1 we can draw the following three conclusions: (1) The ABEEM/MM model

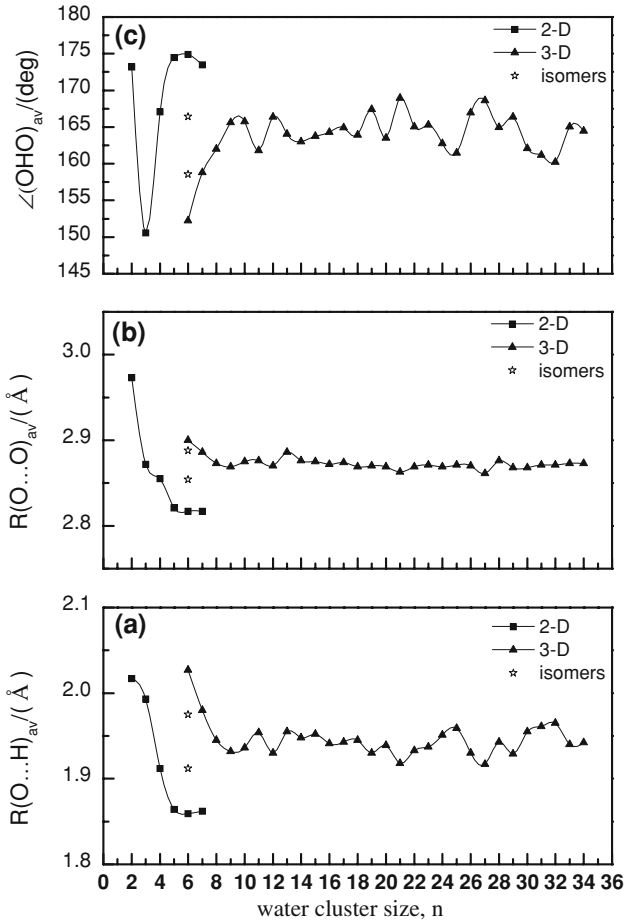

Fig. 6 The transition from 2D to 3D structures at hexamer region predicted by the ABEEM/MM model based on the variation trends of **a** mean values $R(O\cdots H)_{av}$ of the distances between oxygen and H-bonded hydrogen atom, **b** mean values $R(O\cdots O)_{av}$ of the nearest oxygen-oxygen distances, and **c** mean values $\angle(OHO)_{av}$ of the angles of the H-bonded three atoms for the relatively most stable structures of $(H_2O)_n$ (n = 2–34) with respect to the cluster size n

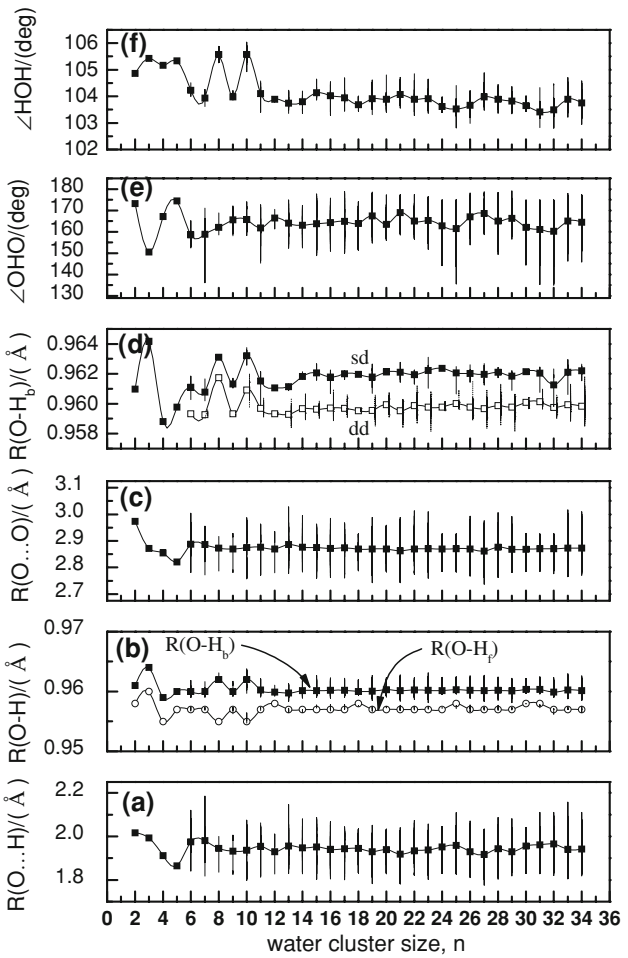

Fig. 7 Variations of **a** the distance R(O···H), **b** the bond length R(O–H), **c** the distance R(O···O), **d** the bond length $R(O–H_b)$, **e** the angle ∠(OHO), and **f** the bend angle ∠(HOH) for the relatively most stable structures of $(H_2O)_n$ (n = 2–34) with increasing cluster size n for the ABEEM/MM model

can fully consider the conformational changes, viz., the charges of all atoms, bonds, and lone-pair electrons can fluctuate according to the different ambient environment. (2) Compared with isolated water, the remarkable change of charges takes place at the position where the hydrogen bond forms. For example, for the "daa" monomer in the structure 17cage_1, one bound H atom (q_{H20} is 0.4714) and two bound lone-pair electrons (q_{lpO19} is −0.2884 and $q_{lp'O19}$ is −0.2780) of O atom exhibit relatively larger absolute charges than the corresponding free H atom (0.2897) and lone-pair electron (−0.1908) of O atom. In the same way, this is also true of "da", "daa", and "ddaa" monomers. (3) The monomer type can be easily identified only from ABEEM charge distributions. For example, the charges q_{H2} and q_{H3} of two H atoms are 0.3978 and 0.4020, respectively, which are larger than the charge 0.2897 of free H atom in isolated water, because the two H atoms are both involved in hydrogen bonds. At the same time, the absolute charges 0.3085 and 0.3045 of two lone-pair electrons (lpO1 and lp′O1) on O atom are larger than the absolute charge 0.1908 of free lone-pair electron on O atom in isolated water, because the two lone-pair electrons are also involved in hydrogen bonds. It is obvious that this water molecule belongs to "ddaa" monomer.

To summarize, the fluctuating charges of the water molecules can quantitatively reflect the redistribution with the changed ambient environment and make a compensation for the shortages of fixed-point charge models. Meanwhile, the fluctuating charges are very important in the calculations of the binding energies and dipole moments.

3.4 Energetic properties of $(H_2O)_n$ (n = 2–34) clusters

With an increase in the size of water clusters, there is an increase in the number of hydrogen bonds and hence an

Table 1 The charges of the relatively most stable structure for $(H_2O)_{17}$ calculated by the ABEEM/MM model

17cage_1	ABEEM/MM	17cage_1	ABEEM/MM	17cage_1	ABEEM/MM	17cage_1	ABEEM/MM
q_{O1}	0.1147	q_{O31}	0.1091	$q_{O13\text{-}H15}$	−0.1507	$q_{lp'O7}$	−0.3268
q_{H2}	0.3978	q_{H32}	0.3702	$q_{O16\text{-}H17}$	−0.1530	$q_{lp'O10}$	−0.2824
q_{H3}	0.4020	q_{H33}	0.3765	$q_{O16\text{-}H18}$	−0.1451	$q_{lp'O10}$	−0.2829
q_{O4}	0.1112	q_{O34}	0.1089	$q_{O19\text{-}H20}$	−0.1453	$q_{lp'O13}$	−0.2703
q_{H5}	0.3834	q_{H35}	0.3804	$q_{O19\text{-}H21}$	−0.1530	$q_{lp'O13}$	−0.2893
q_{H6}	0.3776	q_{H36}	0.3613	$q_{O22\text{-}H23}$	−0.1451	$q_{lp'O16}$	−0.2830
q_{O7}	0.1124	q_{O37}	0.1085	$q_{O22\text{-}H24}$	−0.1530	$q_{lp'O16}$	−0.2730
q_{H8}	0.3880	q_{H38}	0.4405	$q_{O25\text{-}H26}$	−0.1447	$q_{lp'O19}$	−0.2884
q_{H9}	0.3875	q_{H39}	0.2855	$q_{O25\text{-}H27}$	−0.1523	$q_{lp'O19}$	−0.2780
q_{O10}	0.1107	q_{O40}	0.1089	$q_{O28\text{-}H29}$	−0.1504	$q_{lp'O22}$	−0.2819
q_{H11}	0.3742	q_{H41}	0.4555	$q_{O28\text{-}H30}$	−0.1504	$q_{lp'O22}$	−0.2884
q_{H12}	0.3828	q_{H42}	0.2765	$q_{O31\text{-}H32}$	−0.1505	$q_{lp'O25}$	−0.2744
q_{O13}	0.1102	q_{O43}	0.1079	$q_{O31\text{-}H33}$	−0.1502	$q_{lp'O25}$	−0.2754
q_{H14}	0.3837	q_{H44}	0.3665	$q_{O34\text{-}H35}$	−0.1497	$q_{lp'O28}$	−0.2364
q_{H15}	0.3682	q_{H45}	0.3672	$q_{O34\text{-}H36}$	−0.1506	$q_{lp'O28}$	−0.3217
q_{O16}	0.1098	q_{O46}	0.1068	$q_{O37\text{-}H38}$	−0.1455	$q_{lp'O31}$	−0.2425
q_{H17}	0.2758	q_{H47}	0.3676	$q_{O37\text{-}H39}$	−0.1517	$q_{lp'O31}$	−0.3126
q_{H18}	0.4684	q_{H48}	0.3573	$q_{O40\text{-}H41}$	−0.1459	$q_{lp'O34}$	−0.3146
q_{O19}	0.1113	q_{O49}	0.1088	$q_{O40\text{-}H42}$	−0.1525	$q_{lp'O34}$	−0.2358
q_{H20}	0.4714	q_{H50}	0.3705	$q_{O43\text{-}H44}$	−0.1513	$q_{lp'O37}$	−0.2667
q_{H21}	0.2820	q_{H51}	0.3691	$q_{O43\text{-}H45}$	−0.1513	$q_{lp'O37}$	−0.2706
q_{O22}	0.1114	$q_{O1\text{-}H2}$	−0.1509	$q_{O46\text{-}H47}$	−0.1501	$q_{lp'O40}$	−0.2728
q_{H23}	0.4757	$q_{O1\text{-}H3}$	−0.1506	$q_{O46\text{-}H48}$	−0.1506	$q_{lp'O40}$	−0.2697
q_{H24}	0.2813	$q_{O4\text{-}H5}$	−0.1505	$q_{O49\text{-}H50}$	−0.1500	$q_{lp'O43}$	−0.2245
q_{O25}	0.1095	q_{O4H6}	−0.1507	$q_{O49\text{-}H51}$	−0.1505	$q_{lp'O43}$	−0.3145
q_{H26}	0.4553	$q_{O7\text{-}H8}$	−0.1519	q_{lpO1}	−0.3085	$q_{lp'O46}$	−0.2199
q_{H27}	0.2821	$q_{O7\text{-}H9}$	−0.1520	$q_{lp'O1}$	−0.3045	$q_{lp'O46}$	−0.3112
q_{O28}	0.1094	$q_{O10\text{-}H11}$	−0.1505	q_{lpO4}	−0.3194	$q_{lp'O49}$	−0.3135
q_{H29}	0.3720	$q_{O10\text{-}H12}$	−0.1518	$q_{lp'O4}$	−0.2515	$q_{lp'O49}$	−0.2343
q_{H30}	0.3774	$q_{O13\text{-}H14}$	−0.1517	$q_{lp'O7}$	−0.2571		

The geometry is in Fig. 3. q_O and q_H are the charges on the site of the atom O and H, q_{O-H} is the charge on the site of the ratio of covalent atomic radii of the atom O and H, q_{lp} is the charge on the site 0.74 Å from the O atom

increase in the |BE| values, as shown in Fig. 8a and b. The average number of hydrogen bonds ($\bar{n}_H$) per water molecule increases with an increase in n initially but then levels off around 1.8 as n approaches 34. The mean values $\bar{n}_H$ are equal to each other for $(H_2O)_n$ (n = 3–6) clusters, because these geometries (including trimer, tetramer, pentamer, and ring hexamer) are 2D structures.

It seems very attractive to compare the energies of the clusters per hydrogen bond (which are plotted in Fig. 8c) as this information may point toward which structures are favored in the ices and liquid water. There is a noticeable increase in the mean hydrogen-bond strength for n = 2–6. The ring hexamer structure has the highest binding energy per hydrogen bond at 7.47 kcal/mol of all the clusters studied, which is probably of significance when considering the "hexagon rich" structure of the ices. We can also see from Fig. 8c that there does appear to be any sort of convergence after about n = 13 where the mean hydrogen-bond strength is 5.82 kcal/mol. There is perhaps a gradual drift in the energies up to n = 34 (6.52 kcal/mol). Figure 8d describes the relationship between the binding energy per molecule and the cluster size. It shows that the variation of binding energy per molecule exhibits convergence 11.7 kcal/mol at n = 34.

In addition, binding energies of $(H_2O)_n$ (n = 2–22, 24, 28, 32) clusters calculated by the ABEEM/MM model are compared with the previous results obtained from the high-level ab initio calculations at the MP2 level of theory [21, 30, 63], semi-empirical quantum mechanical method [48–52], and empirical potentials [16, 20, 23, 30, 65]. As could be seen from Table 2 the binding energies calculated by the ABEEM/MM potential model are found to be in good

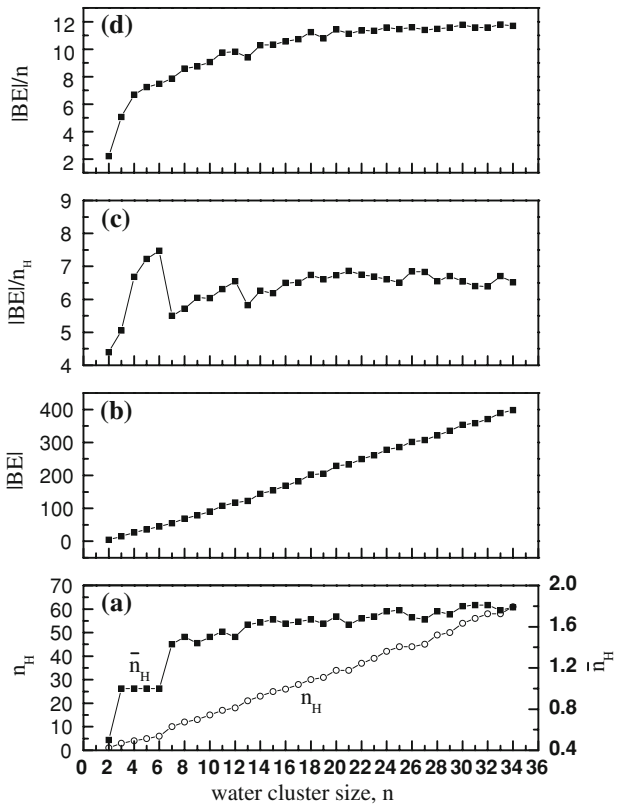

Fig. 8 Variations of **a** the number of hydrogen bonds (n_H) and the average number of hydrogen bonds per water ($\bar{n}_H = n_H/n$), **b** the |BE| value, **c** the hydrogen bond strength (|BE|/n_H), and **d** the binding energy per water (|BE|/n) for the relatively most stable structures of $(H_2O)_n$ (n = 2–34) with an increase in n for the ABEEM/MM model

agreement with those of previous calculations. In a word, the ABEEM/MM potential model can well give rise to and correctly calculate the static properties.

3.5 Dipole moments of $(H_2O)_n$ (n = 2–34) clusters

Of late, there is some controversy in the literature about the "correct" value of the liquid water dipole moment. A recent analysis of X-ray diffraction (XRD) data by the Soper group, which was the first experimental study of the average dipole moment in liquid water, inferred a value of 2.9 D under ambient conditions [100]. Silvestrelli and Parrinello [101] found that the average dipole moment $\langle\mu\rangle$ of water molecule in liquid should be about 3.0 D. The studies of water clusters by Gregory [95] showed that the average dipole moment of a water molecule increased from 2.1 to 2.7 D as the size of the cluster increased from the dimer up to the hexamer. Figure 9a displays the variation trend of the average dipole moments of the relatively most stable structures for $(H_2O)_n$ (n = 2–34) clusters with respect to the cluster size n using the ABEEM/MM model. Concretely, the average dipole moments from monomer to ring hexamer are 1.855, 2.078, 2.329, 2.460, 2.525, and 2.547 D, respectively. This increasing trend in average dipole moments almost gives quantitative agreement with the experiment [7]. The average molecular dipole moments against cluster size are slower to converge toward the predicted liquid water value of 2.80 D with the ABEEM/MM model [82].

Furthermore, there appears to be some significant structure to the values of the dipoles with respect to cluster size. This is most evident in the plot of the total dipole moment against cluster size (Fig. 9b) which exhibits strong maxima at n = 2, 5, 7, 10, 15, 19, 21, 23, 26, 28 and minima at n = 4, 6, 8, 12, 18, 24, 30 (where the dipole moments are close to or identically zero by symmetry). It is interesting to speculate as to why this series closely follows a periodicity of 6 for the minima at n = 12, 18, 24, 30. The n = 12, 18, 24, 30 structures are all built out of stacked ring hexamer units and so it is not surprising they share similar properties.

4 Conclusions

Based on the newly developed flexible-body and charge-fluctuating ABEEM/MM water potential model, we have studied and explored several static properties of water clusters $(H_2O)_n$ in the n = 2–34 size regime with the change in cluster size, including optimal structures, structural parameters, ABEEM charge distributions, binding energies, hydrogen bonds number, hydrogen-bond strengths, dipole moments, and so on.

The results obtained from optimal structures show that the ABEEM/MM model can correctly predict and reflect a series of structural transitions, including the transition from 2D to 3D structures at hexamer region, the transition from cubes to cages at dodecamer $(H_2O)_{12}$, the transition from all-surface to one water-centered structures at $(H_2O)_{17}$, and the transition from one water-centered to two water-centered structures at $(H_2O)_{33}$. The first three structural transitions show good agreement with those obtained from previous work, while the fourth transition is different from that proposed by Hartke [60–62]. It is worth noting that after the second transition, the abundance of pentamers increases with increasing cagelike character for $(H_2O)_n$ (n = 12–16). Subsequently, the structural alternation between interior (n = 17, 19, 21, 23, 26–29) and all-surface (n = 18, 20, 22, 24–25, 30–32) structures is also predicted in the n = 17–32 cluster regime, and this kind of alternation is very similar to the conclusion reached by Xantheas [66], from electronic structure calculations for $(H_2O)_n$, n = 17–21. Moreover, the relatively most stable structures of $(H_2O)_n$ (n = 12, 18, 24, 30) clusters all have the ring hexamers as building units with opposite hydrogen bond orientation and so it is not surprising they have similar total dipole moments.

The results of a systematic investigation of structural parameters, energetic properties, and dipole moments of

Table 2 Binding energies (BE, kcal/mol) for the minima of clusters (n = 2–22, 24, 28, 32) with the ABEEM/MM model, compared with the results of previous calculations

n	Structure code[a]	n_H	ABEEM/MM	Results of previous calulations				
				MP2/CBS	TTM3-F[f]	TTM2-R	TIP4P	ASP-W4
2	Dimer	1	−4.40	−4.98[b]	−5.18	−4.98[g]	−6.24[i]	−4.99[i]
3	Trimer	3	−15.18	−15.8[b]	−15.77	−15.59[g]	−16.73[i]	−15.48[i]
4	Tetramer	4	−26.72	−27.6[b]	−26.82	−27.03[g]	−27.87[i]	−26.95[i]
5	Pentamer	5	−36.13	−36.3[b]	−35.78	−36.05[g]	−36.35[i]	−35.07[i]
6	Ring	6	−44.84	−44.8[b]	−44.29	−44.28[g]		
	Book	7	−44.22	−45.6[b]	−45.17	−45.14[g]		
7	7a	10	−55.03			−56.75[g]	−58.22[i]	−57.89[i]
8	D_{2d}	12	−68.67	−72.9[c]				
	S_4	12	−67.80	−72.8[c]				
9	9A	13	−78.65			−81.77[g]	−82.32[i]	−82.01[i]
10	D_{same}	15	−89.97			−92.87[g]	−93.46[i]	−94.21[i]
11	11D	17	−103.30			−102.93[g]	−103.13[i]	−102.75[i]
12	S_4S_4	20	−110.20			−117.91[g]	−117.81[i]	−117.60[i]
13	13A	21	−122.14			−126.97[g]	−127.38[i]	−126.62[i]
14	14A	23	−144.07			−140.38[g]	−139.34[i]	−140.95[i]
15	15A	25	−154.73			−151.41[g]	−150.18[i]	−151.46[i]
16	$S_4D_{2d}S_4$	28	−158.88			−164.31[g]	−162.81[i]	−163.89[i]
17	17D	29	−167.75			−174.19[g]	−172.99[i]	−172.46[i]
18	18E	31	−188.80			−187.35[g]	−184.81[i]	−187.98[i]
19	19cage_1b	31	−202.64			−199.30[g]	−196.23[i]	−197.99[i]
20	20A	34	−228.77	−217.9/−218.3[d]	−212.3	−212.51[g]	−208.65[i]	−210.83[i]
	20G	35	−214.67	−215.0/−215.4[d]	−210.42		−207.29[c]	−210.69[c]
	20I	36	−209.49	−212.6/−211.7[d]	−211.45	−210.75[h]	−207.80[c]	−210.24[c]
	20cage[c]	30	−190.94	−200.1[d]	−196.93		−197.47[c]	−197.08[c]
21	21D	37	−223.26			−221.70[h]	−219.10[i]	−217.21[i]
22	22B	39	−241.97			−231.77[h]	−228.53[h]	
	22F	39	−238.04			−234.92[h]	−230.44[h]	
	22 J	39	−231.85			−231.47[h]	−227.91[h]	
	22 K	38	−227.41			−234.28[h]	−231.12[h]	
INDO SCF RHF[e]								
24	24cage	36	−247.13	−243				
28	28cage	42	−281.26	−281				
32	32cage	48	−306.64	−311				

[a] Referencing to the Figs. 2, 3, 4, 5

[b] Xantheas et al. [21]

[c] Xantheas and Aprà [30]

[d] Fanourgakis et al. [63]

[e] McDonald et al. [56]: Applying the intermediate neglect of differential overlap self consistent field restricted Hartree–Fock method (INDO SCF RHF) after parameterization for H and O atoms by Khan

[f] Fanourgakis and Xantheas [23]

[g] Burnham aned Xantheas [20]

[h] Kazimirski and Buch [65]

[i] Wales and Hodges [16]

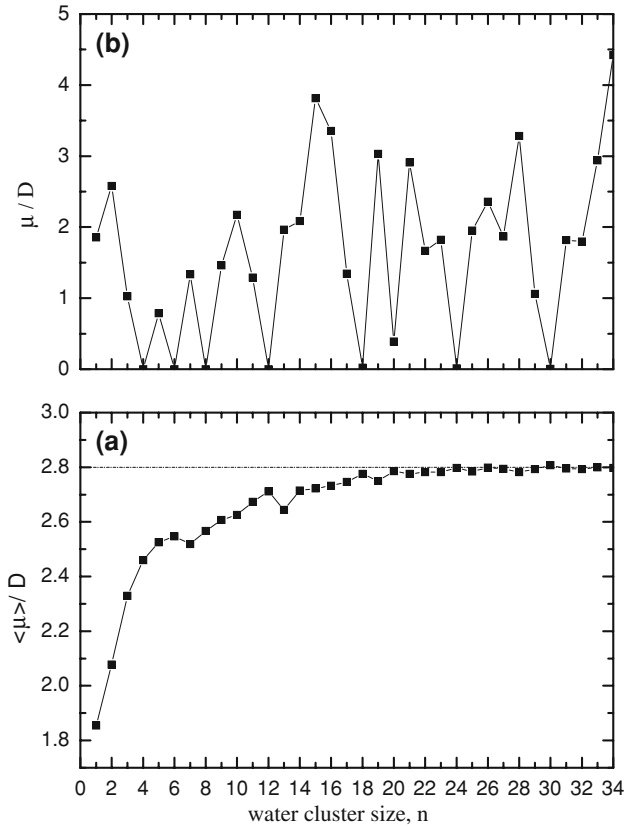

Fig. 9 Average molecular dipole moment and total dipole moment against cluster size for the relatively most stable structures ($n = 1$–34) using the ABEEM/MM model. The *straight line* in **a** shows the calculated average molecular dipole moment in liquid water of 2.80 D with this model

water clusters with increasing cluster size also reflected the objective trait of hydrogen bonds in water cluster system, and provided a strong impetus toward understanding how the water clusters approach the bulk limit.

Recent experimental spectroscopic studies [102] of the IR spectra of the $H^+(H_2O)_n$ ($n = 6$–27) clusters have been successfully obtained, whereas experimental information about neutral water clusters is very little. It is, therefore, hoped that the results of our present study can provide basic clues for further experimental confirmation of neutral water clusters (Fig. 4).

Acknowledgments This research has been aided by a grant from the Youth Science and Technology Innovation Foundation of Shandong Agriculture University in China (No. 23480).

References

1. Liu K, Gruzan JD, Saykally RJ (1996) Science 271:929. doi:10.1126/science.271.5251.929
2. Ludwig R (2001) Angew Chem Int Ed 40:1808. doi:10.1002/1521-3773(20010518)40:10<1808::AID-ANIE1808>3.0.CO;2-1
3. Dyke TR, Mack KM, Muetner JS (1977) J Chem Phys 66:498. and references therein. doi:10.1063/1.433969
4. Curtiss LA, Frurip DJ, Blander M (1979) J Chem Phys 71:2703. doi:10.1063/1.438628
5. Huisken F, Kaloudis M, Kulcke A (1996) J Chem Phys 104:17. doi:10.1063/1.470871
6. Liu K, Brown MG, Carter C, Saykally RJ, Gregory JK, Clary DC (1996) Nature 381:501. doi:10.1038/381501a0
7. Liu K, Brown MG, Saykally RJ (1997) J Phys Chem A 101:8995. doi:10.1021/jp9707807
8. Liu K, Brown MG, Cruzan JD, Saykally RJ (1997) J Phys Chem A 101:9011. doi:10.1021/jp970781z
9. Cruzan JD, Viant MR, Brown MG, Saykally RJ (1997) J Phys Chem A 101:9022. doi:10.1021/jp970782r
10. Viant MR, Cruzan JD, Lucas DD, Brown MG, Liu K, Saykally RJ (1997) J Phys Chem A 101:9032. doi:10.1021/jp970783j
11. Morokuma K, Pedersen L (1968) J Chem Phys 48:3275. doi:10.1063/1.1669604
12. Müller-Dethlefs K, Hobza P (2000) Chem Rev 100:143. doi:10.1021/cr9900331
13. Ugalde JM, Alkorta I, Elguero J (2000) Angew Chem Int Ed 39:717. doi:10.1002/(SICI)1521-3773(20000218)39:4<717::AID-ANIE717>3.0.CO;2-E
14. Nielsen IMB, Seidi ET, Janssen CL (1999) J Chem Phys 110:9435. doi:10.1063/1.478908
15. Kryachko ES (1999) Chem Phys Lett 314:353. doi:10.1016/S0009-2614(99)01100-8
16. Wales DJ, Hodges MP (1998) Chem Phys Lett 286:65. doi:10.1016/S0009-2614(98)00065-7
17. Ren P, Ponder JW (2003) J Phys Chem B 107:5933. doi:10.1021/jp027815+
18. Burnham CJ, Li J, Xantheas SS, Leslie M (1999) J Chem Phys 110:4566. doi:10.1063/1.478797
19. Burnham CJ, Xantheas SS (2002) J Chem Phys 116:5115. doi:10.1063/1.1447904
20. Burnham CJ, Xantheas SS (2002) J Chem Phys 116:1500. doi:10.1063/1.1423942
21. Xantheas SS, Burnham CJ, Harrison RJ (2002) J Chem Phys 116:1493. doi:10.1063/1.1423941
22. Fanourgakis GS, Xantheas SS (2006) J Phys Chem A 110:4100. doi:10.1021/jp056477k
23. Fanourgakis GS, Xantheas SS (2008) J Chem Phys 128:074506. doi:10.1063/1.2837299
24. Wales DJ, Ohmine I (1993) J Chem Phys 98:7245
25. Wales DJ, Ohmine I (1993) J Chem Phys 98:7257. doi:10.1063/1.464717
26. Kim KS, Dupuis M, Kie GC, Clementi E (1986) Chem Phys Lett 131:451. doi:10.1016/0009-2614(86)80564-4
27. Tsai CJ, Jordan KD (1991) J Chem Phys 95:3850. doi:10.1063/1.460788
28. Bink G, Glasser L (1984) J Phys Chem 88:3412. doi:10.1021/j150660a009
29. Maheshwary S, Patel N, Sathyamurthy N, Kulkarni AD, Gadre SR (2001) J Phys Chem A 105:10525. doi:10.1021/jp013141b
30. Xantheas SS, Aprà E (2004) J Chem Phys 120:823. doi:10.1063/1.1626624
31. Gruenloh CJ, Carney JR, Arrington CA, Zwier TS, Fredericks SY, Jordan KD (1997) Science 276:1678. doi:10.1126/science.276.5319.1678
32. Roth W, Schmitt M, Jacoby C, Spangenberg D, Janzen C, Kleinermanns K (1998) Chem Phys 239:1. doi:10.1016/S0301-0104(98)00252-3

33. Buck U, Ettischer I, Melzer M, Buch V, Sadlej J (1998) Phys Rev Lett 80:2578. doi:10.1103/PhysRevLett.80.2578
34. Brudermann J, Melzer M, Buck U, Kazimirski JK, Sadlej J, Buch V (1999) J Chem Phys 110:10649. doi:10.1063/1.479008
35. Sadlej J, Buch V, Kazimirski JK, Buck U (1999) J Phys Chem A 103:4933. doi:10.1021/jp990546b
36. Torchet G, Schwartz P, Farges J, de Feraudy MF, Raoult B (1983) J Chem Phys 79: 6196
37. Torchet G, Farges J, de Feraudy MF, Raoult B (1989) Ann Phys Fr 14:245. doi:10.1051/anphys:01989001402024500
38. Bartell LS, Huang J (1994) J Phys Chem 98:7455
39. Huang J, Bartell LS (1995) J Phys Chem 99:3924
40. Devlin JP, Joyce C, Buch V (2000) J Phys Chem A 104: 1974
41. Devlin JP, Buch V (2003) In: Devlin JP, Buch V (eds) Water in confining geometries, chap 17, Springer, Berlin
42. Delzeit L, Devlin JP, Buch V (1997) J Chem Phys 107:3726. doi:10.1063/1.474728
43. Buch U, Steinbach C (2003) In: Buch V, Devlin JP (eds) Water in confining geometries, chap 3, Springer, Berlin
44. Tsai CJ, Jordan KD (1993) J Phys Chem 97:5208. doi:10.1021/j100122a005
45. Sremaniak LS, Perera L, Berkowitz ML (1996) J Chem Phys 105:3715. doi:10.1063/1.472190
46. Moore Plummer PL (1997) J Mol Struct THEOCHEM 417:35. doi:10.1016/S0166-1280(97)00030-4
47. Kirschner KN, Shields GC (1994) Int J Quantum Chem 28:349. doi:10.1002/qua.560520835
48. Khan A (1995) J Phys Chem 99:12450, and references therein. doi:10.1021/j100033a013
49. Khan A (1996) Chem Phys Lett 253:299
50. Khan A (1996) Chem Phys Lett 258:574
51. Khan A (1997) J Chem Phys 106:5537
52. Khan A (1999) J Phys Chem A 103:1260, and references therein. doi:10.1021/jp983515+
53. Day PN, Pachter R, Gordon MS, Merrill GN (2000) J Chem Phys 112:2063. doi:10.1063/1.480775
54. Farantos SC, Kapetanikis S, Vegiri A (1993) J Phys Chem 97:12158. doi:10.1021/j100149a010
55. Baba A, Tanaka J, Saito S, Matsumoto M, Ohmine I (1998) J Mol Liq 77:95. doi:10.1016/S0167-7322(98)00070-1
56. McDonald S, Ojamäe L, Singer SJ (1998) J Phys Chem A 102:2824. doi:10.1021/jp9803539
57. Nigra P, Kais S (1999) Chem Phys Lett 305:433. doi:10.1016/S0009-2614(99)00423-6
58. Guimaraes FF, Belchior JC, Johnston RL, Roberts C (2002) J Chem Phys 116:8327. doi:10.1063/1.1471240
59. Lee C, Chen H, Fitzgerald G (1995) J Chem Phys 102:1266. doi:10.1063/1.468914
60. Hartke B (2003) Phys Chem Chem Phys 5:275
61. Hartke B (2003) Eur Phys J D 24:57
62. Hartke B (2002) Angew Chem Int Ed 41:1468. doi:10.1002/1521-3773(20020503)41:9<1468::AID-ANIE1468>3.0.CO;2-K
63. Fanourgakis GS, Aprà E, Xantheas SS (2004) J Chem Phys 121:2655. doi:10.1063/1.1767519
64. Bulusu S, Yoo S, Aprà E, Xantheas SS, Zeng XC (2006) J Phys Chem Lett 110:11781
65. Kazimirski JK, Buch V (2003) J Phys Chem A 107:9762. doi:10.1021/jp0305436
66. Lagutschenkov A, Fanourgakis GS, Schatteburg GN, Xantheas SS (2005) J Chem Phys 122:194310. doi:10.1063/1.1899583
67. Plummer PLM, Chen TS (1983) J Phys Chem 87:4190. doi:10.1021/j100244a043
68. Egorov AV, Brodskaya EN, Laaksonen A (2002) Mol Phys 100:941. doi:10.1080/00268970110105406
69. Sediki A, Lebsir F, Martiny L, Dauchez M, Krallafa A (2008) Food Chem 106:1476. doi:10.1016/j.foodchem.2007.03.080
70. Kabrede K, Hentschke R (2003) J Phys Chem B 107:3914. doi:10.1021/jp027783q
71. Berendsen HJC, Grigera JR, Straatsman TP (1987) J Phys Chem 91:6269. doi:10.1021/j100308a038
72. Perera L, Berkowitz ML (1993) J Chem Phys 99:4236. doi:10.1063/1.466234
73. Stillinger FH, David CW (1980) J Chem Phys 73:3384
74. Weber TA, Stillinger FH (1983) J Phys Chem 87:4277
75. Jorgensen WL, Chandrasekhar J, Madura JD, Impey RW, Klein ML (1983) J Chem Phys 79:926. doi:10.1063/1.445869
76. Yang ZZ, Wu Y, Zhao DX (2004) J Chem Phys 120:2541. doi:10.1063/1.1640345
77. Qian P, Yang ZZ (2007) Sci China Ser B 50:190. doi:10.1007/s11426-007-0003-2
78. Li X, Yang ZZ (2005) J Phys Chem A 109:4102. doi:10.1021/jp0458093
79. Zhang Q, Yang ZZ (2005) Chem Phys Lett 403:242. doi:10.1016/j.cplett.2005.01.011
80. Yang ZZ, Zhang Q (2006) J Comput Chem 27:1. doi:10.1002/jcc.20317
81. Yang ZZ, Qian P (2006) J Chem Phys 125:064311. doi:10.1063/1.2210940
82. Wu Y, Yang ZZ (2004) J Phys Chem A 108:7563. doi:10.1021/jp0493881
83. Yang ZZ, Li X (2005) J Phys Chem Lett 109:3517
84. Li X, Yang ZZ (2005) J Chem Phys 122:084514. doi:10.1063/1.1853372
85. Cong Y, Yang ZZ, Wang CS, Liu XC, Bao XH (2002) Chem Phys Lett 357:59. doi:10.1016/S0009-2614(02)00439-6
86. Yang ZZ, Wang CS (1997) J Phys Chem A 101:6315. doi:10.1021/jp9711048
87. Wang CS, Li SM, Yang ZZ (1998) J Mol Struct THEOCHEM 430:191
88. Wang CS, Yang ZZ (1999) J Chem Phys 110:6189. doi:10.1063/1.478524
89. Cong Y, Yang ZZ (2000) Chem Phys Lett 316:324. doi:10.1016/S0009-2614(99)01289-0
90. Yang ZZ, Wang CS (2003) J Theor Comput Chem 2:273. doi:10.1142/S0219633603000434
91. Nocedal J (1980) Math Comput 35:773. doi:10.2307/2006193
92. Eggen BR, Marks AJ, Murrel JN, Farantos SC (1994) Chem Phys Lett 219:247. doi:10.1016/0009-2614(94)87053-5
93. Bai J, Su CR, Parra RD, Zeng XC, Tanaka H, Koga K, Li JM (2003) J Chem Phys 118:3913. doi:10.1063/1.1555091
94. Tanaka H, Yamamoto R, Koga K, Zeng XC (1999) Chem Phys Lett 304:378. doi:10.1016/S0009-2614(99)00293-6
95. Gregory JK, Clary DC, Liu K, Brown MG, Saykally RJ (1997) Science 275:814, and references therein. doi:10.1126/science.275.5301.814
96. Lee HM, Suh SB, Lee JY, Tarakeshwar P, Kim KS (2000) J Chem Phys 112:9759. doi:10.1063/1.481613
97. Bobbert C, Schütte S, Steinbach C, Buck U (2002) Eur Phys J D 19:193
98. Andersson P, Steinbach C, Buck U (2003) Eur Phys J D 24:53
99. Jeffrey GA (1997) An introduction to hydrogen bonding. Oxford University Press, Oxford
100. Badyal YS, Saboungi ML, Price DL, Shastri SD, Haeffner DR, Soper AK (2000) J Chem Phys 112:9206. doi:10.1063/1.481541
101. Silvestrelli PL, Parrinello M (1999) Phys Rev Lett 82:3308. doi:10.1103/PhysRevLett.82.3308
102. Shin JW, Hammer NI, Diken EG, Johnson MA, Walters RS, Jaeger TD, Duncan MA, Christie RA, Jordan KD (2004) Science 304:1137. doi:10.1126/science.1096466